PROGRESS ON THE DESIGN OF THE POLARIZED MEDIUM-ENERGY ELECTRON ION COLLIDER AT JLAB*

F. Lin[#], A. Bogacz, P. Brindza, A. Camsonne, E. Daly, Ya.S. Derbenev, D. Douglas, R. Ent,
D. Gaskell, R. Geng, J. Grames, J. Guo, L. Harwood, A. Hutton, K. Jordan, A. Kimber, G. Krafft,
R. Li, T. Michalski, V.S. Morozov, P. Nadel-Turonski, F. Pilat, M. Poelker, R. Rimmer,
Y. Roblin, T. Satogata, M. Spata, R. Suleiman, A. Sy, C. Tennant, H. Wang, S. Wang, H. Zhang,
Y. Zhang, Z. Zhao, Jefferson Lab, Newport News, VA, USA
P. N. Ostroumov, Argonne National Laboratory, Argonne, IL 60439 USA
D.P. Barber, Deutsches Elektronen-Synchrotron (DESY), 22607 Hamburg, Germany
Yu.M. Filatov, Moscow Inst. of Phys. and Tech., Dolgoprydny, and Joint Inst. for Nucl. Research,
Dubna, Russia
S. Abeyratne, B. Erdelyi, Northern Illinois University, DeKalb, IL 50115 USA
A. Castilla, J. Delayen, C. Hyde, K. Park, Old Dominion University, Norfolk, VA 23529 USA
A. Kondratenko, M. Kondratenko, Sci. & Tech. Laboratory Zaryad, Novosibirsk, Russia
Y. Cai, Y.M. Nosochkov, M. Sullivan, M-H Wang, U. Wienands, SLAC National Accelerator
Laboratory, Menlo Park, CA 94305 USA
J. Gerity, T. Mann, P. McIntyre, N.J. Pogue, A. Sattarov, Texas A&M University, College
Station, TX, USA

Abstract

The Medium-energy Electron Ion Collider (MEIC) at JLab is designed to provide high luminosity and high polarization needed to reach new frontiers in the exploration of nuclear structure. The luminosity, exceeding 10^{33} cm^{-2}s^{-1} in a broad range of the center-of-mass (CM) energy and maximum luminosity above 10^{34} cm^{-2}s^{-1}, is achieved by high-rate collisions of short small-emittance low-charge bunches made possible by high-energy electron cooling of the ion beam and synchrotron radiation damping of the electron beam. The polarization of light ion species (p, d, ^{3}He) can be easily preserved and manipulated due to the unique figure-8 shape of the collider rings. A fully consistent set of parameters have been developed considering the balance of machine performance, required technical development and cost. This paper reports recent progress on the MEIC accelerator design including electron and ion complexes, integrated interaction region design, figure-8-ring-based electron and ion polarization schemes, RF/SRF systems and ERL-based high-energy electron cooling. Luminosity performance is also presented for the MEIC baseline design.

INTRODUCTION

The proposed MEIC at JLab is designed to meet the requirements of science program outlined in the EIC white paper [1]. The overall MEIC design strategies [2,3] towards achieving high luminosity and high polarization have not changed since 2006 but technical design aspects have evolved. In particular, the updates from the 2012 MEIC design report [3] are the results of an ongoing optimization process for performance, cost, technical risk and potential for phasing and future upgrades.

Main changes with respect to the design report in 2012 are given as follows [4].

- Ion and electron collider ring circumferences have been increased from 1.5 to 2.2 km.
- Electron collider ring is designed reusing PEP-II components (magnets, vacuum chambers, RF, etc.).
- Ion collider ring is designed based on super-ferric magnet technology.
- Only one single 8 GeV figure-8 shape booster is needed based on super-ferric magnets.

In this paper, we provide technical descriptions of the main subsystems on the baseline design and present the resulting luminosity performance.

MEIC BASELINE DESIGN

The MEIC is designed to be a traditional ring-ring collider. The central part of this facility is two figure-8 shape collider rings that are vertically stacked and housed in the same underground tunnel, as shown in Fig. 1. The figure-8 crossing angle is 81.7°, partitioning a collider ring into two arcs and two long straights. The ion beam executes a vertical excursion to the plane of electron ring for a horizontal crossing for electron-ion collisions. Two collider rings have nearly identical circumferences of approximately 2.2 km, and fit well in the Jefferson Lab site.
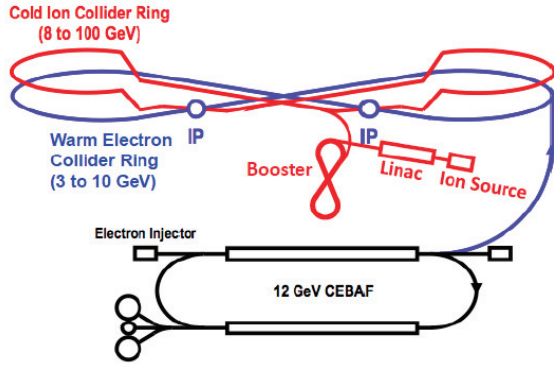
Figure 1: A schematic layout of MEIC complex.

Electron and Ion Complex

Electron complex consists of the CEBAF recirculating SRF linac and electron collider ring. CEBAF serves as a full energy injector to the collider ring and provides up to 12 GeV, high repetition rate and high polarization (> 85%) electron beams. No further upgrade for the beam energy, current and polarization is needed beyond the 12 GeV upgrade. The transfer line between the CEBAF and MEIC electron collider ring is constructed reusing PEP-II Low Energy Ring (LER) dipoles and quadrupoles and designed with $120°$ phase advance FODO cells to ensure no significant emittance growth due to the synchrotron radiation.

The electron collider ring is made of normal conducting magnets reconditioned from the decommissioned PEP-II e^+e^- collider High Energy Ring (HER) at SLAC [5]. The PEP-II vacuum chambers and 476MHz RF systems are also reused in the electron collider. The stored electron beam current is up to 3 A, scaled down when the beam energy exceeds 7 GeV in order to satisfy the limit of 10 kW/m synchrotron radiation power density and 10 MW total radiation power for the PEP-II vacuum chambers.

The ion complex is a new facility, consisting of ion source, linac, booster and collider ring. All required ion species will be generated by two sources, namely, an Atomic Beam Polarized Ion Source (ABPIS) [6] for polarized or un-polarized light ions and an Electron Beam Ion Source (EBIS) [7] or Electron Cyclotron Resonance (ECR) ion source [8] for un-polarized heavy ions up to lead. The ion pulse from the source will be accelerated to 285 MeV for protons and 112 MeV/u for lead ions by a lina consisting of both warm and cold RF cavities. A SRF ion linac developed at ANL as a heavy ion accelerator [9] is very effective in accelerating a wide variety of ions from H$^-$ to lead ion $^{208}Pb^{67+}$ and can be adopted in the MEIC with minimum changes. The 8 GeV booster ring is designed to avoid transition crossing for all ion species during the acceleration, and utilize multi-turn injection with combined longitudinal and transverse painting and charge exchange mechanism.

The ion collider ring accelerates protons from 8 to up to 100 GeV or ions in the equivalent energy rang and stores a beam energy of 20 to 100 GeV for protons or up to 40 GeV/u for heavy ions. The ion collider ring is shaped to make a 50 mrad crossing angle with the electron beam at the collision points and match the electron ring footprint [10]. Both ion booster and collider ring are designed using new super-ferric magnets [11], a cost-effective type of superconducting magnet with modest field strength (up to 3 T) in both construction and operation.

Detector Region Design

MEIC's primary detector [3] is designed to provide essentially full acceptance to all fragments produced in collisions. Figure 2 shows a complete 3D model of the full-acceptance detector region using GEANT4-based G4beamline [12] and GEMC [13]. The forward hadron detection is done in three stages: (1) fragments with scattering angles down to a few degree are detected in a 2 m long end-cap, (2) fragments up to a few degree are detected after passing through a 1 m long 2 Tm spectrometer dipole in front of the final focusing quads (FFQs), and (3) fragments up to about one degree pass through the apertures of the FFQs and are detected in a 4 m space before and a 16 m space after a second 4 m long 20 Tm spectrometer dipole. On the forward electron side, the large-angle reaction products are detected in the second end-cap. Electron scattered at small angles are detected in a low-Q^2 tagger consisting of large-aperture electron FFQs and a spectrometer dipole with a few meters of instrumented space on either side.
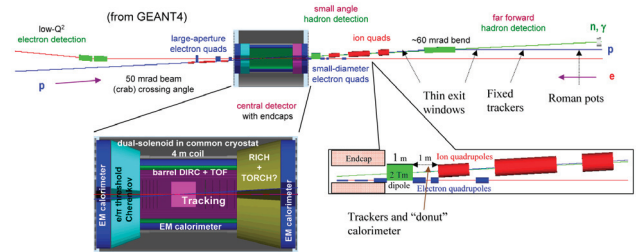

Figure 2: 3D model of the full-acceptance detector region in GEANT4-based G4beamline and GEMC.
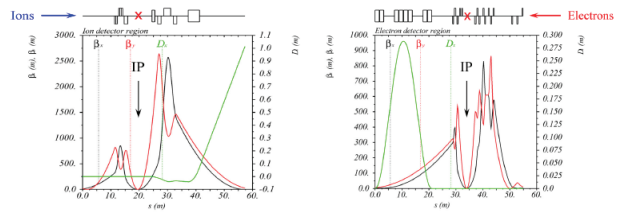

Figure 3: Optics of ion (left) and electron (right) detector regions.

The interaction region optics shown in Fig. 3 is optimized to meet the detection requirements [14, 15, 16]. In particular, the detector space is made asymmetric by leaving a large 7 m distance from the IP to the first ion FFQ in the downstream ion direction where the reaction products tend to go, while having the upstream ion FFQs placed closer to the IP at 3.5 m to minimize their chromatic contribution. In addition, as shown in Fig. 3, both ion and electron beams are focused again towards the

ends of the elements-free spaces downstream of the respective spectrometer dipoles to allow closer placement of the detectors at those locations, which enhances momentum resolution of the forward detector in combination with the relatively large dispersion values. The simulations [14] have shown that the far-forward detection system is capable of accepting (1) neutrals in a cone with a full angle of about 25 mrad down to zero degree, (2) recoil baryons with up to 99.5% of the beam energy for all scattering angles, and (3) recoil baryons with scattering angle down to 2-3 mrad for all energies.

Ion and Electron Polarization

The figure-8 geometry of the MEIC rings is an elegant way to preserve and control the polarization during the acceleration and collision. Precession of spin in one arc is exactly cancelled in the other so that the net spin rotation is zero and spin tune is energy independent of beam energy. This means that there is no preferred direction of the polarization and spin orientation is easily controlled and stabilized by using relatively small magnetic fields.

In the ion booster of MEIC, a weak solenoid stabilizes the polarization in the longitudinal direction in the straight where it is placed [17, 18, 19, 20]. There is no problem with ramping the field of such solenoid during the acceleration cycle. The required solenoid field integral does not exceed 0.7 Tm at the top energy of the booster for both protons and deuterons. It provide sufficient spin tune shift of 0.01 and 0.003 from zero for protons and deuterons, respectively.

The beam polarization of any particle (p, d, 3He, …) is controlled in the ion collider ring using universal 3D spin rotators [18, 19, 20] located at the end of the experimental straight for the ion polarization control. The rotator consists of three modules for control of the radial, vertical and longitudinal components of the polarization (see Fig. 4). The module for control of the radial (vertical) polarization component consists of two pairs of opposite-field solenoids and three vertical (radial)-field dipoles producing a fixed orbit bump. To keep the orbit bumps fixed, the field of vertical- and radial-field dipoles must be ramped proportionally to the beam momentum. The module for control of the longitudinal polarization component consists of a single weak solenoid. Such 3D spin rotator can provide any desired polarization at the IP. The maximum required dipole and solenoid magnetic field strengths are 3 and 3.6 T, respectively. The spin tunes are shifted from zero by sufficient amounts of 0.01 and $2.5 \cdot 10^{-4}$ for proton and deuteron, respectively. Another same type of the 3D spin rotator can be used for compensation of the zero-integer resonance strength, which substantially reduces the required field integral of the 3D rotator solenoids [20].
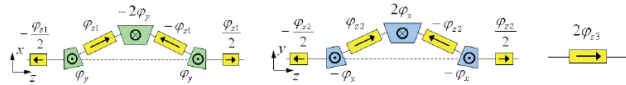

Figure 4: Modules for control of the radial (left), vertical (middle) and longitudinal (right) spin components.

Comprehensive strategies have been developed to preserve and control the electron polarization in the MEIC [21]. In particular, the electron polarization in the collider ring is designed to be vertical in the arcs to minimize spin diffusion (depolarization) and longitudinal at the IP for physics experiments. Proper spin orientation is accomplished using universal spin rotators [22] located at each end of two arcs. These spin rotators, composed of interleaved solenoids and dipoles, are designed to rotate electron polarization in the entire energy range and leave the orbit intact. The polarization configuration in the MEIC electron collider ring is determined by the solenoid field directions in the pair of spin rotators in the same long straight [21, 23]. These were chosen to have opposite solenoid polarities, as shown in Fig. 5. Then the polarization is anti-parallel to the vertical guiding field in one arc and parallel to the guiding field in the other one, regardless of the choice of two opposite longitudinal polarizations at the IPs (purple solid and dashed arrows in Fig. 5). Therefore, the Sokolov-Ternov self-polarization [24] process has a net depolarization effect integrated over the whole collider ring, and both polarization states from the polarized source will be equally affected.
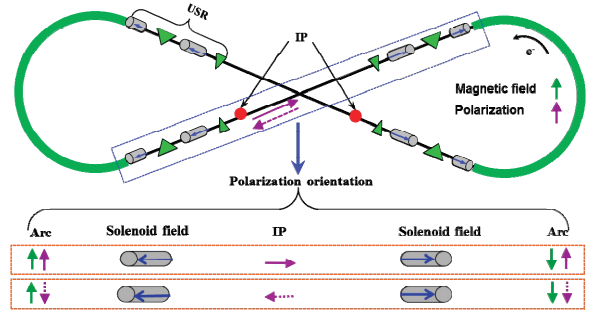

Figure 5: Polarization configuration in the MEIC electron collider ring. Solenoid fields (blue arrows) in two spin rotators in the same straight have opposite directions.

In addition, with oppose longitudinal solenoid fields in the pair of spin rotators in the same long straight, the net field integral is zero. As a result, the 1st order spin perturbation in the solenoids for off-momentum particles vanishes [23]. This significantly extends the polarization lifetime and reduces the burden on the spin matching and ring-optics design. Though this polarization configuration has zero equilibrium polarization, with highly polarized injected beams, the estimated polarization lifetimes at various energies in Table 1) are adequate for detectors to collect data.

Table 1: Estimated Electron Polarization Lifetime at Various Energies

Energy (GeV)	Estimated Pol. Lifetime (hours)
3	66
5	5.2
7	2.2
9	1.3
10	0.86

Ion Beam Cooling

MEIC baseline design utilizes conventional well-developed electron cooling [25] for cooling the ion beam. The design adopts a scheme of multi-phase cooling [26, 27] during formation of the ion beam and during collision for enhancing the cooling efficiency.

Table 2 summarizes the cooling phases in the MEIC, consisting of DC cooling in the booster and Bunched Beam (BB) ERL-based cooling in the collider ring. Electron cooling is first called in the booster ring for assisting accumulation of positive ions (from helium-3 $^3He^{2+}$ to partially-stripped lead ion $^{208}Pb^{32+}$) injected from the ion linac. For the proton or deuteron beams, MEIC utilizes a H-/D- negative ion source so no cooling is required in this accumulation state. The accumulated proton beam is boosted to 2 GeV kinetic energy, the initial cooling is performed at this energy and the transverse emittance is reduced to the design values. The proton beam is then boosted to 7.9 GeV and transferred to the collider ring. Electron cooling is used again in the collider ring during stacking of the proton beam transferred (in 8 batches), and is continued after the beam is accelerated to the collision and during e-p collisions. In these two stages, electron cooling is for suppressing the IBS induced emittance growth and maintaining the emittance to the design values. Cooling of ion beams will follow a similar plan according to ion beam energies in the booster and collider rings.

Table 2: MEIC Multi-Phased Electron Cooling

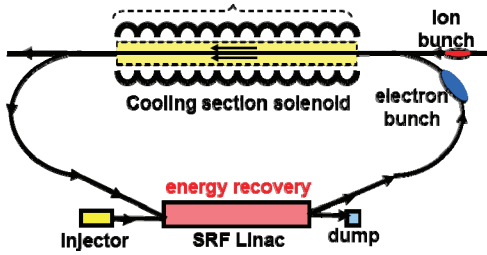|	Phase	Function	Proton kinetic energy (Gev/u)	Electron kinetic energy (MeV)	Cooler type
Booster	1	Assisting accumulation of injected positive ions	$0.11 \sim 0.19$	$0.062 \sim 0.1$	DC
	2	Emittance reduction	2	1.09	
Collider ring	3	Suppressing IBS and maintaining emittance during stacking of beams	7.9	4.3	BB (ERL)
	4	Suppressing IBS and maintaining emittance during collision	100	55	

Figure 6: Schematic drawing of a bunched beam cooler based on an ERL, with upgrade circulator ring connection in green.

The recently built and commissioned 2 MeV DC electron cooler for the COSY at FZ-Juelich (Germany) [28] can be readily adopted in the MEIC booster with only minor modifications. In the MEIC baseline design, a single pass ERL cooling is applied. Current gun and SRF capability allow the energy recovered linac beam to provide enough electron cooling. Figure 6 shows a schematic drawing of a bunched beam cooler based on an ERL technology.

RF/SRF System

Multiple pulses from the ion linac will be captured and accumulated in the booster using a low frequency RF system with a harmonic number of 1. The tunable RF system will track the revolution frequency during the energy ramping process. At 8 GeV the stored bunch will be transferred to the collider ring and captured by a similar RF system with harmonic number 8. Once the filling is complete the stored and cooled beam will be ramped to collision energy, again with the frequency being tuned to keep up with the revolution frequency.

At the collision energy, the ion beam will be re-bucketed into a high frequency bunching RF system at 952 MHz. High RF voltage gradient will be required to achieve the desired short bunch length. The system will employ all new sing-cell HOM damped SRF cavities, left in Fig. 7, in a new modular cryostat based on previous JLab technology. The RF input power requirements are lower than the electron collider ring because there is no synchrotron radiation power, but the HOM extracted power is significant due to the high stored beam current and short bunches. The bunch frequency will initially be 476 MHz to match the electron ring PEP-II RF system. The ion beam will be pre-bunched by a single modest 476 MHz station (e.g. one spare PEP-II cavity) before the 952 MHz system is turned on. The 952 MHz RF system will provide double bunch repetition rate in the future for the luminosity upgrade.
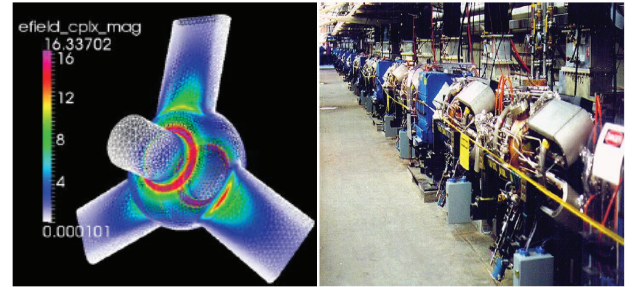

Figure 7: (Left) HOM damped SRF ion cavity concept. (Right) PEP-II NCRF systems installed in the tunnel.

PEP-II 476 MHz normal conducting RF (NCRF) system [29], right in Fig. 7, was designed to supply up the 10 MW of synchrotron radiation power, present a very low impedance to the beam, safely dissipate many kW of HOM power per cavity and operate with very high reliability. This NCRF system perfectly satisfies the MEIC electron collider ring requirements and is available to populate along the ring (34 copper cavities, 13 1.2 MW klysrons and ancillary equipment). For future high luminosity and high energy upgrades, new 952 MHz SRF cavities can be installed alongside or in place of the existing copper systems. This gives a seamless path to upgrade and manage the graceful phase out of the PEP-II systems as they eventually age.

The deflecting crabbing cavity concept in the MEIC is similar to those being developed for the LHC [30]. These cavities also need to be HOM-damped and operated at a relatively low frequency to minimize the effects of curvature on the bunches. 952 MHz cavities will fulfil these requirements and be compatible with future upgrades.

The ERL in the electron cooler requires an SRF linac cryomodule containing four 5-cell cavities and short booster cryomodule containing four single-cell cavities. These all need HOM damping to achieve the desired high current and would use similar ancillary components to the ion ring RF system.

LUMINOSITY PERFORMANCE

The MEIC nominal parameters at three representative design points in the low, medium and high CM energy regions respectively are presented in Table 3. The luminosity is above 10^{33}cm^{-2}s^{-1} in all these design points for the full-acceptance detector, and reaches 4.6×10^{33}cm^{-2}s^{-1} at the medium CM energy of approximately 45 GeV. For the second detector, the interaction region design can be optimized for reaching a higher luminosity, ~ 60% increase, while still retaining a fairly large detector acceptance. Figure 8 illustrates the general trends of the MEIC luminosity in the whole CM energy region for both full acceptance and high luminosity detectors.

Table 3: MEIC Nominal Design Parameters for a Full-Acceptance Detector

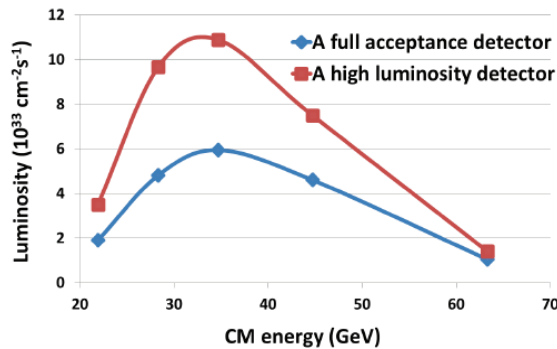| CM energy	GeV	21.9 (low)		44.7 (medium)		63.3 (high)	
		p	e	p	E	p	e
Beam energy	GeV	30	4	100	5	100	10
Collision frequency	MHz	476		476		159	
Particles per bunch	10^{10}	0.66	3.9	0.66	3.9	2.0	2.8
Beam current	A	0.5	3	0.5	3	0.5	0.72
Polarization	%	>70	>70	>70	>70	>70	>70
Bunch length, RMS	cm	2.5	1.2	1.0	1.2	2.5	1.6
Norm. emittance, vert. / horz.	μm	0.5/0.5	74/74	1/0.5	144/72	1.2/0.6	1152/576
Horizontal and vertical β^*	cm	3/1.2	5/2	2/4 (1.6/0.8)	2.6/1.3 (1.6/0.8)	5/2.5 (2/1)	2.4/1.2 (1.6/0.8)
Vert. beam-beam parameter		0.01	0.02	0.006 (0.004)	0.014 (0.021)	0.002 (0.001)	0.013 (0.021)
Laslett tune-shift		0.055	small	0.01	small	0.01	small
Detector space	m	3.6/7 (4.5/4.5)	3/3.2 (3/3)	3.6/7 (4.5/4.5)	3/3.2 (3/3)	3.6/7 (4.5/4.5)	3/3.2 (3/3)
Hour-glass (HG) reduction factor		0.89 (0.67)		0.89 (0.74)		0.73 (0.58)	
Lumi./IP, w/HG correction, 10^{33}	cm^{-2}s^{-1}	1.9 (3.5)		4.6 (7.5)		1.0 (1.4)	

Figure 8: Luminosity of e-p collisions in the MEIC.

At the low energies, space charge of the low energy ion beam severely limits the bunch charge, particularly for short bunches in the MEIC. The design strategy is to allow a longer bunch length (2.5 cm) than that at higher energy, thus accommodating the full bunch charge while remaining the design limit for the Laslett space charge tune-shift of 0.06. However, there is non-negligible loss of luminosity (11%) due to the hourglass effect. A traveling-focusing scheme [31] is considered to recover the hourglass effect induced luminosity loss.

At the high energies, synchrotron radiation of the electron beam is the dominating effect. The electron beam current must be scaled down proportionally to the 4th power of the electron energy to reduce the synchrotron radiation power to an acceptable level of 10 MW in the whole energy range. The design strategy is to choose a relatively low bunch repletion rate and boost the bunch charge proportionately. Accordingly, the proton bunch length must be increased to alleviate single bunch effects. This results a significant luminosity loss due to the hourglass effect. Mismatching the colliding beam spot sizes at the IP, by taking advantage of very weak beam-beam interaction, can be applied to compensate the luminosity loss.

At the medium energies, the strong beam-beam effect dominates the MEIC luminosity. An optimum luminosity can be achieved by combing a high bunch repetition rate, small beam emittance and small β^* at the IP. This energy region delivers the highest luminosity in the MEIC.

CONCLUSION

MEIC design strategies towards high luminosity and high polarization have not changed in the past 10 years. The baseline design is the results of optimization of machine performance, project cost, technical risk assessment and potential for future upgrades. This paper reports technical descriptions of the main subsystems and some key design aspects in the MEIC complex. The baseline design of MEIC based on a ring-ring concept is mature and can deliver luminosity from a few 10^{33} to a few 10^{34} cm^{-2}s^{-1} and polarization over 70% in a broad CM energy range with low technical risks.

REFERENCES

[1] A. Accardi et al., EIC white paper, arXiv:1212.1701, (2012) .
[2] A. Afanasev et al., edited by Ya.S Derbenev, L. Merminga and Y. Zhang, http://web.mit.edu/eicc/DOCUMENTS/ELIC-ZDR-20070118.pdf. (2007).
[3] S. Abeyratne et al., MEIC Design Report, edited by J. Bisognano and Y. Zhang, arXiv:1209.0757, (2012).
[4] S. Abeyratne et al., MEIC Design Summary for NSAC EIC Cost Estimate Sub-Committee, edited by G. A. Krafft, submitted to arXiv (2015).
[5] F. Lin et al., in this proceeding, TUPTY084 (2015).
[6] T. Clegg et al., NIM A, Vol.357, Issues 2-3, p.200-211 (1995).
[7] J. Alessi et al., Proc. of the LINA-2006, p.385 (2006).

[8]   R. Geller, Annual Review of Nuclear and Particle Science, Vol.40, 15-44 (1990).

[9]   B. Mustapha et al., Proc. of PAC'07, p.581 (2003).

[10]   V.S. Morozov et al., in this proceeding, TUPWI031 (2015).

[11]   F.R. Huson et al., IEEE Trans. Nucl. Sci. NS-32, 3462 (1985).

[12]   G4beamline, http://g4beamline.muonsinc.com

[13]   GEMC simulation framework, http://gemc.jlab.org

[14]   V.S. Morozov et al., Proc. of IPAC'12, TUPPR080, p.2011 (2012).

[15]   F. Lin et al., Proc. of IPAC'13, TUPAC28, p.508 (2013).

[16]   V.S. Morozov et al., Proc. of IPAC'14, MOPRO005, p.71 (2014).

[17]   A.M. Kondratenko et al., PoS (PSTP 2013) 026 (2013).

[18]   A.M. Kondratenko et al., EIC'14, to be published (2014).

[19]   A.M. Kondratenko et al., Proc. of IPAC'14, MOPRO004, p.68 (2014).

[20]   A.M. Kondratenko et al., SPIN'14, to be published (2014).

[21]   F. Lin et al., Proc. of IPAC'14, MOPRO006, p.74 (2014).

[22]   P. Chevtsov et al., JLab-TN-10-026 (2010).

[23]   F. Lin et al., PoS (PSTP 2013) 025 (2013).

[24]   A.A. Sokolov et al., Sov. Phys. Dokl. 8: 1203 (1964).

[25]   G.I. Budker, Proc. of the Intern. Symp. on Electron and Positron Storage Rings, p.II-I-I (1966); Atomnaya Energia, 22, 346 (in Russian) (1967).

[26]   Y.S. Derbenev et al., Proc. of COOL'07 Workshop, THAP12 (2007).

[27]   Y.S. Derbenev et al., Proc. of COOL'09 Workshop, FRM2MCCO01 (2009).

[28]   "COSY Electron Cooling Conceptual Design Report", BINP (2009).

[29]   J.T. Seeman, Proc. EPAC'08, TUXG01, p.946 (2008)

[30]   S.U. De Silva et al., Proc. of IPAC'13, WEPWO080, p.2483 (2013).

[31]   V. Balakin, Travelling focus, LC-91 (1991).